PERGAMON

Journal of Structural Geology 22 (2000) 373–382

JOURNAL OF STRUCTURAL GEOLOGY

www.elsevier.nl/locate/jstrugeo

Boudinage in multilayered rocks under layer-normal compression: a theoretical analysis

Nibir Mandal[a], Chandan Chakraborty[b,*], Susanta Kumar Samanta[a]

[a]*Department of Geological Sciences, Jadavpur University, Calcutta 700032, India*
[b]*Geological Studies Unit, Indian Statistical Institute, 203, B.T. Road, Calcutta 700035, India*

Received 22 June 1999; accepted 27 September 1999

Abstract

This paper presents a dynamic analysis of boudinage in multilayers of alternate brittle and ductile layers under layer-normal compression. Based on the mode of fracturing of individual brittle layers, boudinage is classified into three types: *tensile fracture boudinage* (Type 1), *shear fracture boudinage* (Type 2a) and *extensional shear fracture boudinage* (Type 2b). The layer-thickness ratio, T_r ($= t_b/t_d$), and the strength ratio, F ($= T/2\eta\varepsilon$), between the brittle and the ductile units are the principal physical factors determining the type of boudinage. Type 1 boudinage develops rectangular boudins and occurs when T_r is low (< 4.5) or F is high (> 0.8). In contrast, Type 2a boudinage takes place when T_r is high (> 8.5) or F is low (< 0.5). The intermediate values of these factors delimit the field of extensional shear fracture boudinage. The square of fracture spacing or boudin width in Type 1 boudinage is linearly proportional to layer-thickness, whereas that in Type 2 boudinage shows a non-linear relationship with layer-thickness. The aspect ratio (A_r) of all the types of boudins is inversely proportional to layer-thickness ratio (T_r). However, Type 1 and Type 2 boudins, have contrasting aspect ratios, which are generally greater and less than 1, respectively.

1. Introduction

Boudinage structure is a common extensional features, especially in rocks with a layering of contrasting lithologies. Comparable structures, described as foliation boudins (Hambrey and Milnes, 1975), are also observed in homogeneous foliated rocks, apparently showing no competence contrast (Coe, 1959; Platt and Vissers, 1980). The development of foliation boudins is attributed to the presence of pre-existing fractures (Platt and Vissers, 1980; Mandal and Karmakar, 1989) or interlocking pinching-and-swelling instability (Cobbold et al., 1971). Recently, Kidan and Cosgrove (1996) have demonstrated that during layer-normal compression extensional structures of different orders develop sequentially in the multilayer, similar to the development of different orders of folds in multilayers under progressive layer-parallel shortening.

The classical rectangular boudins (Lohest, 1909; Corin, 1932; Wegmann, 1932; Ramberg, 1955) are considered to develop by tensile fracturing of brittle layers at right angles to layering and where the layers suffer little or no ductile deformation before or after rupturing. This is also supported by the mechanical models on tensile failure of brittle objects embedded in a ductile matrix (Hobbs, 1967; Lloyd and Ferguson, 1981; Lloyd et al., 1982; Masuda and Kuriyama, 1988; Ji et al., 1997; Ji and Saruwatari, 1998).

Tensile fracture boudins may also assume rhomboidal shape, if the brittle units in the multilayer make an angle with the bulk tension direction or are deformed by layer-parallel simple shear. In such cases tensile fractures form oblique to the layering, giving rise to rhomboidal boudins (Strömgard, 1973). Other workers have shown that the rhomboidal shape may be the result of post-boudinage deformation of rectangular

* Corresponding author.
E-mail addresses: nibir@jugeo.clib0.ernet.in (N. Mandal), chandan@isical.ac.in (C. Chakraborty).

0191-8141/00/$ - see front matter
PII: S0191-8141(99)00156-X

boudins due to a layer-parallel shear component (Ghosh and Ramberg, 1976; Hanmer, 1986).

Field observations suggest that in many cases the rhomboidal shape of boudins may be linked to development of parallel shear fractures in the competent layers oblique to the layering (Cloos, 1947; Griggs and Handin, 1960; Uemura, 1965; Gay and Jaeger, 1975). The boudins in such cases may assume a trapezoidal shape if the shear fractures are non-parallel, forming a horst-and-graben geometry. A domino-type structure results when the rhombic boudins undergo rotation and offsetting during progressive layer-parallel extension (Freund, 1974; Garfunkel and Ron, 1985; Gaudemar and Tapponier, 1987; Jordan, 1991). Analogue model experiments (Karmakar and Mandal, 1989; Mandal and Khan, 1991) indicate that the orientation and the spacing of parallel oblique-fractures in the brittle layer are the principal physical factors that could control the kinematics of rhombic boudins.

It is thus understood that boudinage involves both tensile and shear fracturing of the competent units in a multilayer. Rock deformation experiments (Griggs and Handin, 1960; Paterson, 1978; Hirth and Tullis, 1994) indicate that tensile fracturing occurs at low confining pressure, whereas shear fracturing prevails at relatively high confining pressure. However, such a correlation may not hold for a natural system. For example, shear fracture and tensile fracture boudins are often observed in the field at a single outcrop or even a hand specimen (e.g. fig. 17.1 in Ghosh, 1994), suggesting that the two modes of fracturing may prevail at the same confining pressure. Apparently, in addition to confining pressure, there appear to be other factors governing the mode of fracturing of brittle layers (cf. Talbot, 1970).

Under layer-normal compression of multilayers, extensional features develop affecting the individual layers as well as the entire multilayer in the course of progressive deformation (Kidan and Cosgrove, 1996). In certain circumstances closely spaced competent layers may respond to the stress as a whole and rupture by through-going fractures, a phenomenon that corresponds more to faulting than boudinage (Lloyd, 1999, personal communication). The purpose of the present paper, however, is to investigate theoretically the mechanical basis of different styles of first order boudinage (i.e. fracturing of brittle layers as single units) affecting the individual layers of a multilayer, in relation to mode of fracturing under layer-normal compression. A few experiments were performed on multilayer models of plasticine (brittle) and putty (ductile) under layer-normal compression to test the theoretical model. Based on the mode of fracturing of individual brittle layers, three different types of boudinage have been recognized: (1) tensile fracture boudinage (Type 1), giving rise to rectangular boudins, (2) shear fracture boudinage (Type 2a), producing rhombic or trapezoidal boudins without any intervening separation zone, and (3) extensional shear fracture boudinage (Type 2b), forming rhombic or trapezoidal boudins with intervening separation zones (Fig. 1). The study also reveals that each type of boudinage produces boudins with a characteristic range of aspect ratios.

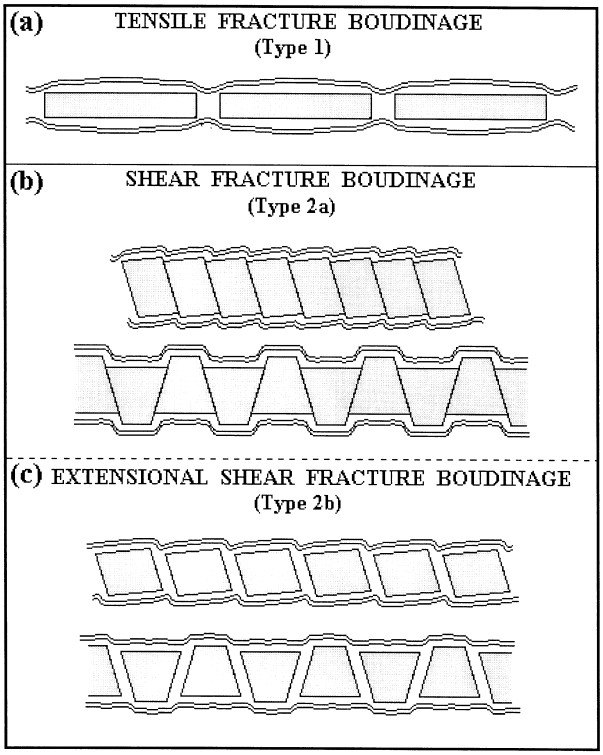

Fig. 1. A genetic classification of different types of boudins formed under layer-normal compression.

2. Theoretical considerations

2.1. Mechanical model

Modeling of fracture development in a stiff layer embedded by a softer medium hinges on the formulation of stress transfer to the stiff layer from the matrix. The different models as used in the mechanics of composite materials and applied to geological systems (Ramberg, 1955; Hobbs, 1967; Lloyd et al., 1982; Pollard and Segall, 1987; Ji et al., 1997; Ji and Saruwatari, 1998) include (1) the shear-lag model, (2) the stress-perturbations model and (3) the energy balance model (see Ji et al., 1998 for a review of these models and references).

In the present analysis, the mechanical model is framed to represent boudinage of a multilayer with alternate competent (brittle) and incompetent (ductile)

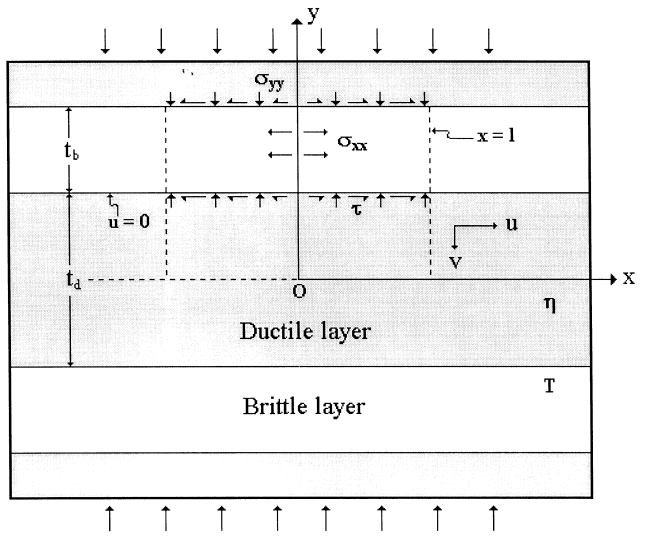

Fig. 2. Geometrical and kinematic considerations for the dynamic analysis of boudinage of a brittle unit in a multilayer under layer normal compression (big arrow). Small arrows indicate traction components of the flow in the ductile layer to the brittle layer. u and v are the velocity components of the flow in the ductile unit. The traction components σ, τ on the brittle unit are shown for an arbitrarily chosen layer-segment of length $2l$ (within vertical dashed lines). T and η are the tensile strength of the brittle layer and the co-efficient of viscosity of the ductile layer, respectively.

layers of uniform thickness under layer-normal shortening (Fig. 2). The incompetent units are modeled with a Newtonian viscous rheology. The bulk deformation is considered to be a pure shear with an overall extension parallel to layering. The transfer of stress to the competent unit from the incompetent medium is formulated with the shear-lag model (Ramberg, 1955). Ji et al. (1998) have shown that deformation of a multilayer can take place with or without interface-slip. In our model, we assume that there is no slip at the interfaces between the brittle and ductile units. In addition, the model is idealized by assuming that the layer-normal shortening occurs mostly in the ductile unit and the change in layer thickness of the brittle unit is negligibly small. During deformation the flowing ductile material exerts tangential and normal traction to the surfaces of the brittle layers (Fig. 2) that, under specific conditions, may eventually lead to boudin formation, the type of boudins being determined by the mode of fracturing of the brittle layers. We adopt the Griffith criterion for the dynamic analysis of failure of brittle layers (cf. Hancock, 1985). According to the Griffith criterion, the tensile stress σ_{xx} and the compressive stress σ_{yy} in brittle layers have to satisfy the following conditions for failure (Jaeger, 1969):

$$\sigma_{xx} = T, \quad \text{when } \sigma_{yy} + 3\sigma_{xx} > 0 \tag{1a}$$

$$(\sigma_{xx} - \sigma_{yy})^2 + 8T(\sigma_{xx} + \sigma_{yy}) = 0, \quad \text{when } \sigma_{yy} + 3\sigma_{xx} < 0 \tag{1b}$$

where T is the tensile strength of brittle layer. Eqs. (1a) and (1b) represent the conditions for tensile and shear failure, respectively.

In the next section we present the mathematical derivations of the tensile and the compressive stresses on the brittle layers in a multilayer, following the approaches adopted by earlier workers (e.g. Ramberg, 1955; Mandal et al., 1994; Ji et al., 1997).

2.2. Mathematical derivation

Let t_b and t_d be the thicknesses of brittle and ductile units, respectively. We choose a Cartesian coordinate, xy, with the x-axis located along the central line of the ductile layer between any two brittle layers (Fig. 2). The multilayer is deformed under pure shear with the principal shortening normal to layering. In a non-slip boundary condition the instantaneous velocity at all points on the brittle–ductile interface ($y = t_d/2$) assumes a constant value. The velocity components along x and y directions are given by $u = 0$ and $v = \varepsilon t_d/2$, respectively, where ε is the rate of bulk shortening of the ductile unit. The velocity functions for the flow in the ductile unit, that satisfy the above mentioned boundary conditions have the following expressions (Jaeger, 1969):

$$u = \frac{3}{2}\varepsilon x \frac{(t_d^2 - 4y^2)}{t_d^2} \tag{2a}$$

$$v = \frac{1}{2}\varepsilon y \frac{(4y^2 - 3t_d^2)}{t_d^2}. \tag{2b}$$

To find the stresses in the brittle unit, induced by the flow in the ductile material, we require the strain-rate components in the ductile layer. Differentiating Eqs. (2a) and (2b), we have:

$$e_{xx} = \frac{\delta u}{\delta x} = \frac{3}{2}\varepsilon \frac{t_d^2 - 4y^2}{t_d^2} \tag{3a}$$

$$e_{yy} = \frac{\delta v}{\delta y} = \frac{3}{2}\varepsilon \frac{4y^2 - t_d^2}{t_d^2} \tag{3b}$$

$$e_{xy} = \frac{1}{2}\left(\frac{\delta u}{\delta y} + \frac{\delta v}{\delta x}\right) = -6\varepsilon \frac{xy}{t_d^2}. \tag{3c}$$

Eq. (3c) shows that the flow in the viscous layer develops a layer-parallel shear, and thereby exerts a shear stress on the surface of the brittle layer (Fig. 2). The shear stress at any point on the layer interface, i.e. at

$y = t_d/2$, is:

$$\tau = 2\eta e_{xy}, \tag{4}$$

η is the coefficient of viscosity of the ductile material. The shear stresses are symmetrically disposed on either side of the brittle layer, which, as a consequence, suffers a tensile stress (Fig. 2). We now arbitrarily choose a layer segment within $x = -l$ and l (Fig. 2). Under the condition of dynamic equilibrium:

$$t_b \cdot \sigma_{xx} = 2\int_0^l \tau \, dx \tag{5}$$

where σ_{xx} is the tensile stress at $x = 0$. After substituting τ from Eq. (4), Eq. (5) becomes:

$$\sigma_{xx} = \frac{4\eta}{t_b}\int_0^l e_{xy} \, dx. \tag{6}$$

Replacing e_{xy} by Eq. (3c) and after some rearrangements, we have

$$\sigma_{xx} = 6\eta\varepsilon\frac{l^2}{t_b t_d}. \tag{7}$$

The above equation is the expression for the tensile stress in the brittle layer, which is similar to that shown by Ramberg (1955).

Brittle layers in the multilayer also experience a compressive stress from the reaction to the flow in the enclosing viscous layers. We determine the compressive stress on brittle layers in the following way. The rate of energy required for the deformation of an infinitesimal volume in the ductile layer is:

$$dE = 2\eta(e_{xx}^2 + e_{yy}^2 + 2e_{xy}^2)\, dx\, dy. \tag{8}$$

The energy required per unit time, to induce ductile flow in the layer segment in between $x = 0$ and l is then:

$$E = 2\eta\int_0^{t_d/2}\int_0^l (e_{xx}^2 + e_{yy}^2 + 2e_{xy}^2)\, dx\, dy. \tag{9}$$

Substituting the strain components from Eq. (3) into Eq. (9), we have

$$E = \frac{9\eta\varepsilon^2}{t_d^4}\int_0^{t_d/2}\int_0^l \left[(t_d^2 - 4y^2)^2 + (4xy)^2\right] dx\, dy. \tag{10}$$

The solution of Eq. (10) is:

$$E = \frac{6\eta\varepsilon^2}{t_d} l\left(\frac{2}{5}t_d^2 + \frac{1}{3}l^2\right). \tag{11}$$

If the compressive load on the brittle layer is σ_{yy}, the rate of work required for bulk shortening in the ductile layer is:

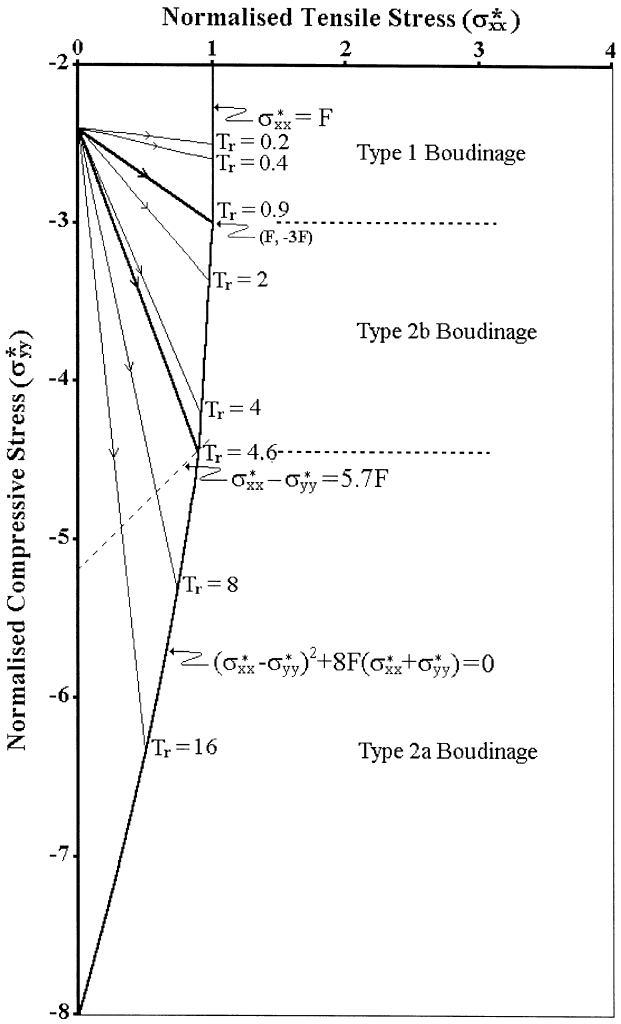

Fig. 3. Analysis of failure in the stress space. The bold line is the failure curve obtained from the Griffith failure criterion. Lines with arrows show variations of the tensile stress and the compressive stress in the brittle layer with increase in l/t_b. T_r is the corresponding layer-thickness ratio in the multilayer. The bold lines with arrows at $T_r = 0.9$ and 4.6 delimit the three types of boudinage.

$$E_b = \frac{1}{2}\sigma_{yy} l\varepsilon t_d. \tag{12}$$

Making an energy balance between Eqs. (11) and (12), we get the magnitude of compressive stress:

$$\sigma_{yy} = 12\eta\varepsilon\left(\frac{1}{3}\frac{l^2}{t_d^2} + \frac{2}{5}\right). \tag{13}$$

The analysis reveals that both the tensile and the compressive stresses on the brittle layer are functions of the length of the layer segment under consideration. For a critical value of l, the stresses in Eqs. (7) and (13) meet the failure criterion (Eq. 1a and b), and result in rupturing of the brittle layer. The failure takes place by tensile fracturing if the stresses satisfy Eq. (1a) of the Griffith criterion. On the other hand, if

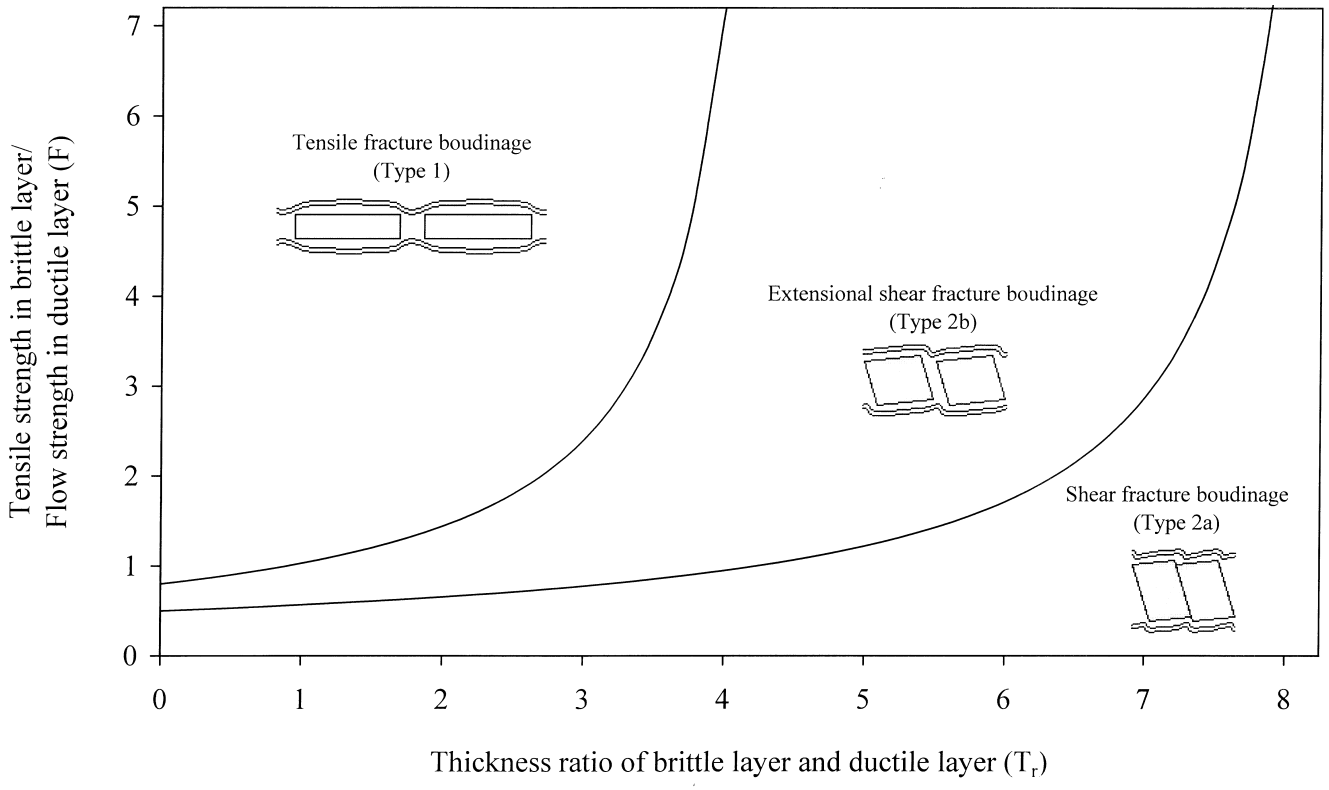

Fig. 4. Fields of the three types of boudinage in the space between layer-thickness ratio and strength ratio in a multilayer. $p^* = 0$.

the stresses fulfil the condition of Eq. (1b), the failure will occur either by shear fracturing or extensional shear fracturing.

2.3. Fields of three types of boudinage

In the analysis of mode of brittle failure we rewrite Eqs. (1a), (1b), (7) and (13), for convenience, in terms of dimensionless quantities as:

$$\sigma^*_{xx} = F \tag{14a}$$

$$(\sigma^*_{xx} - \sigma^*_{yy})^2 + 8F(\sigma^*_{xx} + \sigma^*_{yy}) = 0 \tag{14b}$$

and

$$\sigma^*_{xx} = -p^* + 3A_r^2 T_r \tag{15a}$$

$$\sigma^*_{yy} = -p^* - \frac{2}{5}(6 + 5A_r^2 T_r^2) \tag{15b}$$

where $A_r = l/t_b$, $T_r = t_b/t_d$ and $\sigma^*_{xx} = \sigma_{xx}/2\eta\varepsilon$, $\sigma^*_{yy} = \sigma_{yyx}/2\eta\varepsilon$, $p^* = p/2\eta\varepsilon$. F is the ratio of the tensile strength of the brittle unit to the flow strength of the ductile unit, and is designated as a rheological factor in the subsequent discussion. In Eqs. (15a) and (15b) we add bulk confining pressure, p, as the failure takes place in response to the total stress (deviatoric stress + isotropic stress).

In the σ^*_{xx}–σ^*_{yy} stress space, the failure condition of Eq. (14a) (i.e. tensile failure) defines a straight-line segment, whereas that of Eq. (14b) (i.e. shear failure) describes a parabolic line segment (Fig. 3). These two line segments together delimit the field of stability from that of failure, and meet each other at the point $(F, -3F)$. This, in other words, means that if $\sigma^*_{yy} > -3F$ the failure is by tensile fracturing and if $\sigma^*_{yy} < -3F$ the failure is by shear fracturing. It can be shown from Eq. (14b) that the stress condition on the parabolic failure curve, marking the transition between extensional shear failure and shear failure, will satisfy the condition: $(\sigma^*_{xx} - \sigma^*_{yy}) = 5.7F$. The bottom line is that there are three different segments in the failure curve defining three regimes of failure: tensile failure, shear failure and extensional shear failure.

Eqs. (15a) and (15b) show that layer-thickness ratio controls the tensile and the compressive stresses on the brittle layer. For a given layer-thickness ratio T_r, with increase in A_r the changes in the compressive and tensile stresses describe a linear regression in the stress space. The line meets the failure curve at a critical value of A_r (Fig. 3). The gradient of the regression line increases with increasing layer-thickness ratio. A regression line, therefore, meets one of the three regimes

of the failure curve depending on the layer-thickness ratio.

The layer-thickness ratio in the multilayer that marks the transition between Type 1 and Type 2 boudinage is obtained from Eqs. (15a and b) as:

$$(T_r)_{T/E} = \frac{3}{2}\frac{(3F - p^* - 2.4)}{(p^* + F)}. \quad (16)$$

Similarly, the transition between Type 2b and 2a boudinage is marked by:

$$(T_r)_{E/S} = \frac{3}{2}\left(\frac{4.8F - p^* - 2.4}{0.85F + p^*}\right). \quad (17)$$

Eqs. (16) and (17) delimit the fields of the three types of boudinage in T_r–F space (Fig. 4). The equations reveal that tensile fracture boudinage is possible when $T_r < 4.5$ and $F > 0.8$. In contrast, shear fracture boudinage may take place at all ranges of T_r if $F < 0.5$, or at all ranges of F if $T_r > 8.5$. Extensional shear fracture boudinage, on the other hand, occurs when T_r is less than 8.5 and $F > 0.5$. In general, tensile fracture boudinage is favored at relatively smaller values of layer-thickness ratio, and is progressively replaced by extensional shear fracture boudinage and shear fracture boudinage with increasing layer-thickness ratio in the multilayer. This explains occurrence of different types of boudins in layers of different thicknesses in a single multilayer over an outcrop or hand specimen. It also appears from Fig. 4 that in multilayers with little mechanical contrast ($F < 0.8$) between individual layers, the dominant mode of deformation would be through shear fracturing irrespective of layer-thickness ratio. The theoretical result is consistent with the experimental observations of Kidan and Cosgrove (1996) as well as of the present study.

2.4. Experimental observations

To verify the control of layer-thickness ratio on the mode of boudinage in individual brittle layers we also conducted a series of experiments with analogue physical models. The models consisted of alternate layers of commercially available plasticine (brittle unit) and putty (ductile unit). The interfaces between the plasticine and putty layers were smeared with kerosene oil to prevent interlayer slip during deformation. We deformed the model by a layer-normal compression in a pneumatically driven vertical piston machine. The model was confined by two parallel, vertical glass plates, fixed by two horizontal pistons, and it was allowed to extend in one horizontal direction. A number of experiments were performed on multilayers with different layer-thickness ratios. Models with a layer thickness ratio of 0.15 were observed to be boudinaged by tensile fractures, giving rise to rectangular boudins (Fig. 5a). In contrast, models with a layer-thickness ratio of 2.6 showed rupturing of the brittle layers dominantly by shear fractures (Fig. 5b). In the domains of parallel shear fractures, the boudins underwent rotation and offsetting, giving rise to a typical domino structure, while in the domains of non-parallel shear fractures normal slip along the oppositely dipping fractures produced a horst-and-graben structure (Fig. 5c). For moderate layer-thickness ratios, boudinage was often associated with extensional shear fractures, producing separation zones between the boudins.

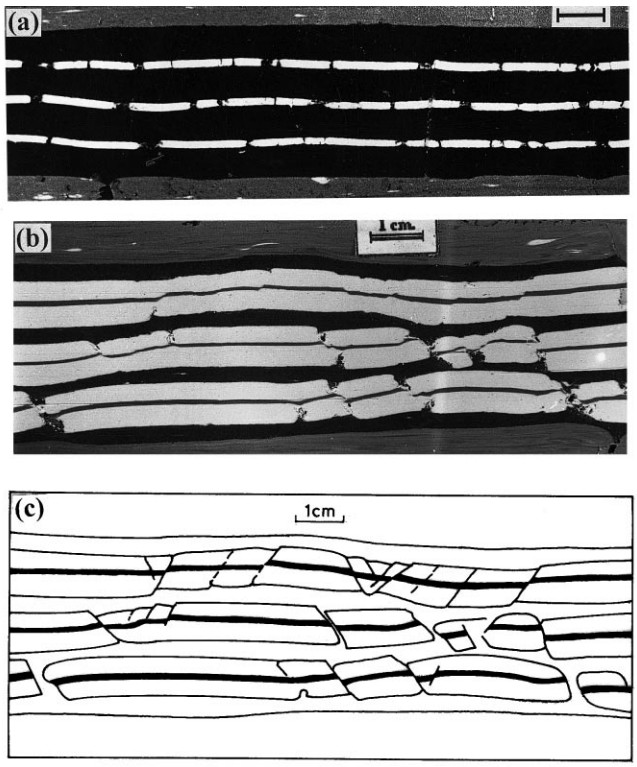

Fig. 5. Boudinage structures in physical models. (a) Tensile fracture boudins. (b) Shear fracture boudins. Models were deformed by vertical compression from the top. Scale bar = 1 cm. (c) Sketch of the deformed model shown in (b); note that the shear fractures are restricted within individual brittle layers, and often occur as conjugate sets (see top layer), indicating that the brittle layers have ruptured as single units; the sense of slip on the shear fractures is consistent with the layer-parallel extension.

2.5. Aspect ratio of boudins

For a given layer-thickness ratio in the multilayer, the compressive stress and the tensile stress in the brittle layer reach the failure condition for a particular ratio between the length of the layer-segment and the thickness of the brittle layer ($l/t_b = A_r$). This ratio represents the dominant aspect ratio of boudins in a brittle layer. From Eqs. (16) and (17), we have in the regime of Type 1 boudinage:

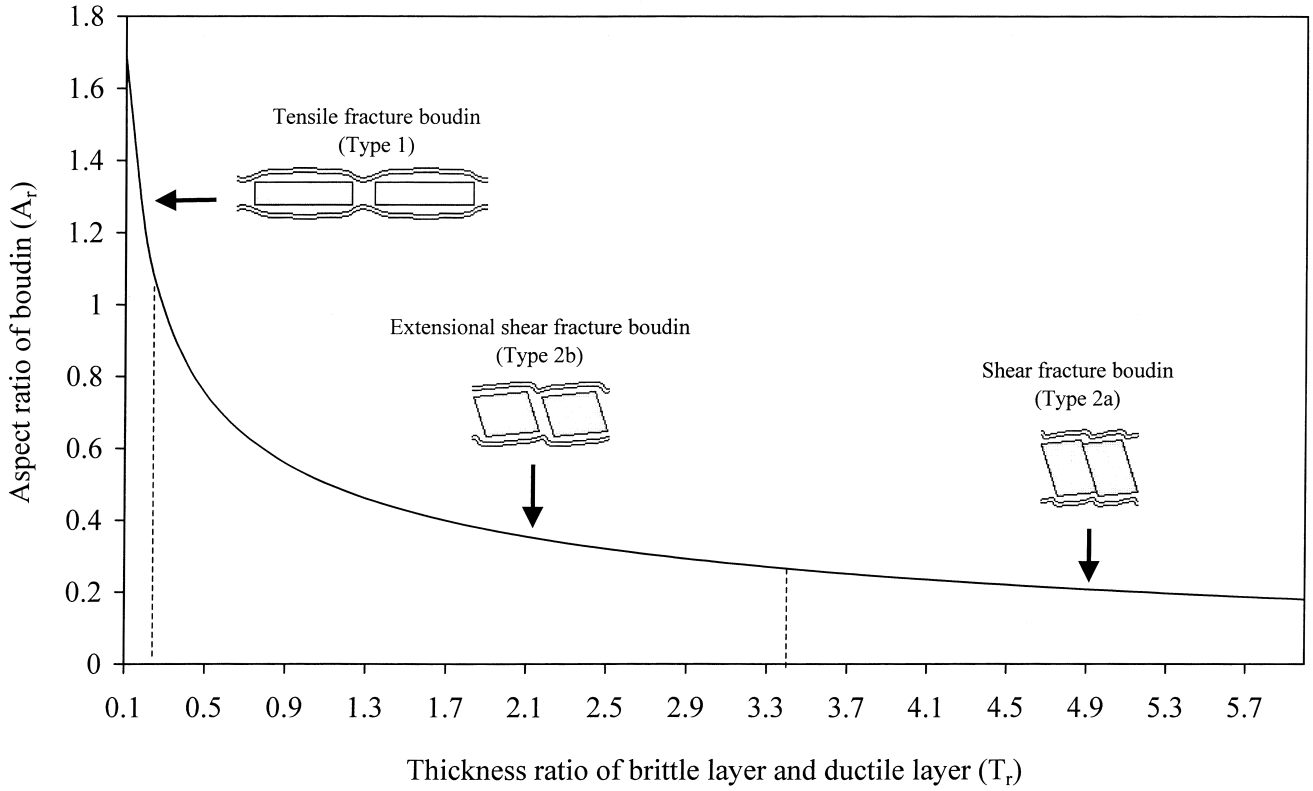

Fig. 6. Variation of aspect ratio of boudin with layer-thickness ratio. Rheological factor $F = 0.9$.

$$A_r^2 = \frac{1}{3}\frac{p^* + F}{T_r}; \tag{18}$$

and in the regime of Type 2 boudinage:

$$A_r^2 = \frac{1}{T_r}\left(\frac{\sqrt{b^2 - 4ca} - b}{2a}\right), \tag{19}$$

where

$$a = [2T_r + 3]^2$$

$$b = \frac{8}{5}\left[9 + 15F + 2(3 - 5F)T_r\right]$$

$$c = \frac{16}{25}\left[9 - 5F(5p^* + 6)\right].$$

Eqs. (18) and (19) show that, irrespective of the mode of boudinage, the aspect ratio of the boudin is inversely proportional to the layer-thickness ratio in the multilayer; however, the aspect ratio of Type 1 boudins decreases more strongly with increasing layer thickness ratio than that of Type 2 boudins (Fig. 6). The equations also reveal that the different types of boudins observed in a multilayer of fairly uniform mechanical contrast between layers are likely to have characteristic ranges of aspect ratios. Tensile fracture boudinage will be favored by relatively thinner layers and the boudins will have relatively large aspect ratios generally greater than 1 (Fig. 6) (e.g. fig. 1.8 in Ramsay and Huber, 1987). In contrast, shear fracture boudinage would prevail in relatively thicker layers and the boudins will have relatively low aspect ratios, generally less than 1 (Fig. 6). This is consistent with natural and experimental observations (Jordan, 1991; Mandal and Khan, 1991). Extensional shear fracture boudins, however, will have intermediate values of aspect ratio.

The theoretical results indicate that the aspect ratio of tensile fracture boudins is more sensitive to both layer-thickness ratio and mechanical contrast between layers in the multilayer than shear fracture and extensional shear fracture boudins (Figs. 6 and 7). However, the aspect ratio of both types of boudins becomes less dependent on the rheological factor with increasing layer thickness ratio (Fig. 7).

2.6. Implications of the theoretical results for the relationship between layer-thickness and fracture spacing

It must now be clear that the boudin width, as modeled in this paper, essentially represents the spacing of the fractures developing within the brittle layers in a multilayer in the process of boudinage. The relation-

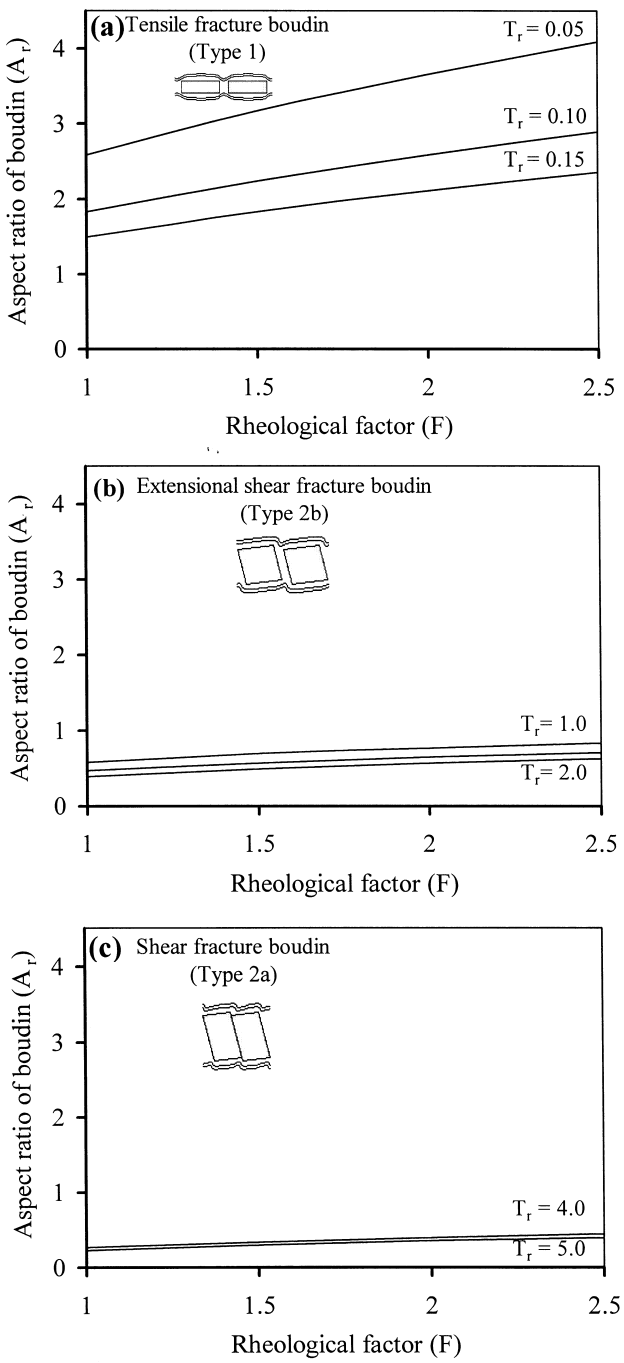

Fig. 7. Plots of aspect ratio of boudins vs. rheological factor in multilayer. T_r is the layer-thickness ratio. (a) Tensile fracture boudins. (b) Extensional shear fracture boudins. (c) Shear fracture boudins.

ship between layer-thickness and fracture spacing has been an area of major interest to material scientists including the earth scientists. Several types of relationships have been obtained using different stress transfer models (Hobbs, 1967; Pollard and Segall, 1987; Souffaché and Angelier, 1989; Mandal et al., 1994; Ji and Saruwatari, 1998). However, these studies mainly deal with tensile fractures. The analysis presented in this paper can be utilized to understand the relationship between layer-thickness and fracture spacing, not only for tensile (Mode 1) fractures but also for shear (Mode 2) fractures. For tensile fractures the relationship can be deduced from Eqs. (7) and (14a) as:

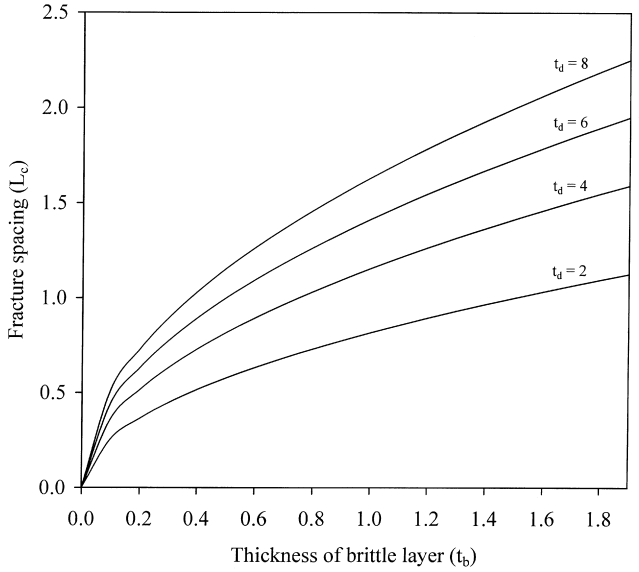

Fig. 8. Variation of spacing of tensile fractures with thickness of brittle layer. t_d is the thickness of ductile layer. $F = 1$.

$$L_c^2 = \frac{1}{3} F t_b t_d, \quad \text{where } F = \frac{T}{2\eta\varepsilon}. \tag{20}$$

In Eq. (20) the factor F, a dimensionless quantity, is simply the ratio between the tensile strength of the brittle material and the flow strength of the ductile material with viscous rheology. The rheological factor defined by Ji and Saruwatari (1998) in their model based on elastic rheology, on the other hand, is a complex function of the elastic constants. Nevertheless, the relationship between fracture spacing and layer thickness remains similar in both the models. Eq. (20) suggests that the width of boudins is linearly proportional to $\sqrt{t_b t_d}$. This is consistent with equation (26) of Ji and Saruwatari (1998), obtained from shear-lag model.

For a fixed value of F, the spacing of tensile fractures is controlled by two parameters: the thickness of the brittle layer (t_b) and the thickness of the ductile layer (t_d). For a constant thickness of ductile layers in the multilayer, fracture spacing is a function of the square root of the thickness of the brittle layer (Fig. 8), as shown in earlier models (Mandal et al., 1994; Ji and Saruwatari, 1998). However, the spacing becomes progressively insensitive to variation in layer-thickness as the intervening ductile layers become thinner and thinner (Fig. 8). This has been well illustrated in the field examples documented by Ladeira and Price (1981).

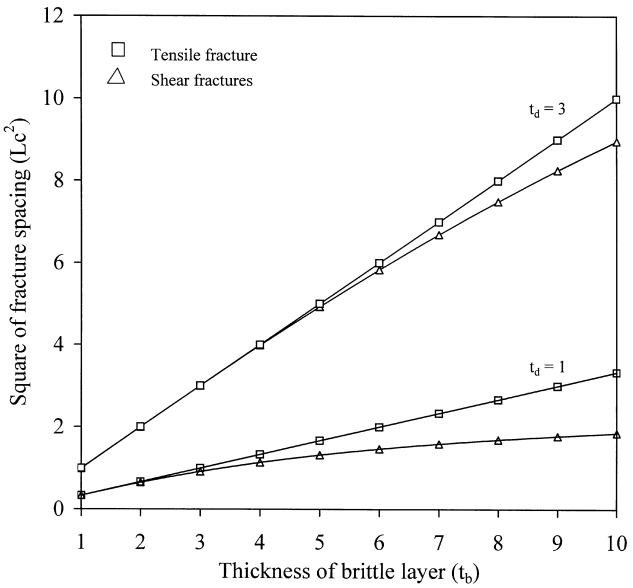

Fig. 9. Plot of square of fracture spacing (L_c^2) vs. thickness of brittle layer (t_b). t_d = thickness of ductile layer. Note that: (1) the spacing of tensile and shear fractures shows linear and non-linear variations respectively, (2) for any layer-thickness the spacing of shear fractures is less than that of tensile fractures, and (3) with decrease in layer-thickness of the ductile unit (t_d), the spacing of shear fractures becomes more insensitive to layer-thickness than that of tensile fractures.

It may be noted that the relationship between fracture spacing (L_c) and layer-thickness (t_b) as discussed above, holds only for tensile (Mode 1) fractures and is likely to be different if the fracturing is by shear failure. The spacing of shear (Mode 2) fractures, derived from Eqs. (7), (13) and (14b), is given by:

$$\left[L_c^2\left(\frac{3}{t_b}+\frac{2}{t_d}\right)+\frac{12}{5}t_d\right]^2+8Ft_d\left[L_c^2\left(\frac{3}{t_b}-\frac{2}{t_d}\right)-\frac{12}{5}t_d\right]=0 \quad (21)$$

It is important to note that, whereas the square of fracture spacing in Type 1 boudinage in Eq. (20) is linearly proportional to layer-thickness (t_b) in the multilayer, that in Type 2 boudinage in Eq. (21) varies nonlinearly with the layer-thickness (Fig. 9). The variation of fracture spacing in Type 2 boudinage shows a decreasing gradient with increasing layer-thickness. Thus, the square of spacing of shear fractures becomes less sensitive to layer-thickness when the latter is large. In addition, with decrease in thickness of ductile layers (t_d), the spacing of shear fractures becomes more insensitive to layer-thickness than that of tensile fractures.

In L_c^2–t_b space, for any layer-thickness of the brittle layer, the spacing of shear fractures is less than that of tensile fractures. Both Mode 1 and Mode 2 fractures lower their spacing as the thickness of the intervening ductile layers is decreased. But the spacing of Mode 2 fractures shows larger departures, and tends to be independent of the thickness of brittle layer (Fig. 9).

3. Conclusions

The outcome of the present paper is summarized along the following points. (1) The type of boudinage in multilayered rocks is controlled largely by the layer-thickness ratio and the mechanical contrast between the brittle and ductile units. (2) Multilayers with low layer-thickness ratios (< 4.5) are virtually boudinaged by tensile fracturing, while those with large layer-thickness ratios (> 8.5) by shear fracturing of the brittle layers (Fig. 4). For moderate layer-thickness ratios, boudinage is likely to be by extensional shear fracturing. (3) The square of boudin width or fracture spacing in tensile fracture boudinage is linearly proportional to layer-thickness, whereas that in shear fracture boudinage is non-linearly proportional to layer-thickness (Fig. 9). (4) The aspect ratio of tensile fracture boudins tends to be greater than 1. In contrast, the aspect ratio of shear fracture boudins is relatively low, generally less than 1 (Fig. 6). (5) In a layered sequence with variable thickness of brittle layers, the aspect ratio of tensile fracture boudins may show a wide scatter, but that of shear fracture boudins in a similar situation will not vary significantly (Fig. 6). (6) The assumptions made in the present analysis are: (i) there is no interlayer slip, (ii) the brittle layer is flawless, homogeneous and isotropic in mechanical properties, (iii) the ductile layers have a constant flow strength, and (iv) the incompetent medium is of Newtonian rheology. These assumptions need to be eliminated in future studies for an improved approximation of the natural observations.

Acknowledgements

We wish to thank Drs. S. Ji and G. E. Lloyd for reviewing the manuscript critically and suggesting many improvements. We are grateful to Dr. R. J. Lisle for giving us an outline for revising the manuscript. The present work was carried out under a project of DST, India sanctioned to NM. CC acknowledges the infrastructural facilities provided by the Indian Statistical Institute, Calcutta.

References

Coe, K., 1959. Boudinage structures in West Cork, Ireland. Geological Magazine 96, 191–200.

Corin, F., 1932. Apropos du boudinage en Ardenne. Bulletin of Geological Society of Belgium 42, 101–117.
Cloos, E., 1947. Boudinage. Transactions of the American Geophysical Union 28, 626–632.
Cobbold, P.R., Cosgrove, J.W., Summers, J.M., 1971. Development of internal structures in deformed anisotropic rocks. Tectonophysics 12, 23–53.
Freund, R., 1974. Kinematics of transform and transcurrent faults. Tectonophysics 21, 93–134.
Garfunkel, Z., Ron, H., 1985. Block rotation and deformation by strike-slip faults. The properties of a type of macroscopic discontinuous deformation. Journal of Geophysical Research 90, 8589–8602.
Gaudemar, Y., Tapponier, P., 1987. Ductile and brittle deformation in the northern Snake Range, Neveda. Journal of Structural Geology 9, 159–180.
Gay, N.C., Jaeger, J.C., 1975. Cataclastic deformation of geological materials in matrices of differing composition: II Boudinage. Tectonophysics 27, 323–339.
Ghosh, S.K., Ramberg, H., 1976. Reorientation of inclusions by combination of pure shear and simple shear. Tectonophysics 34, 1–70.
Ghosh, S.K., 1994. Structural Geology: Fundamental and Modern Developments. Pergamon Press, London.
Griggs, D.T., Handin, J., 1960. Observations on fracture and a hypothesis of earthquakes. In: Griggs, D.T., Handin, J. (Eds.), Rock Deformation (a symposium), Memoirs of the Geological Society of America 79, pp. 347–364.
Hambrey, M.J., Milnes, A., 1975. Boudinage in glacier ice—some examples. Journal of Glaciology 14, 383–393.
Hancock, P.L., 1985. Brittle microtectonics: principles and practices. Journal of Structural Geology 7, 437–457.
Hanmer, S., 1986. Asymmetrical pull-aparts and foliation fish as kinematic indicators. Journal of Structural Geology 8, 111–122.
Hirth, G., Tullis, J., 1994. The brittle–plastic transformation to experimentally deformed quartz aggregates. Journal of Geophysical Research 11, 731–747.
Hobbs, D.W., 1967. The formation of tension joints in sedimentary rocks: an explanation. Geological Magazine 104, 550–556.
Jaeger, J.C., 1969. Elasticity, Fracture and Flow. Methuen, London.
Ji, S., Zhao, P., Saruwatari, K., 1997. Fracturing of garnet crystals in anisotropic rocks during uplift. Journal of Structural Geology 19, 603–620.
Ji, S., Saruwatari, K., 1998. A revised model for the relationship between joint spacing and layer thickness. Journal of Structural Geology 20, 1495–1508.
Ji, S., Zhu, Z., Wang, Z., 1998. Relationship between joint spacing and bed thickness in sedimentary rocks: effects of interbed slip. Geological Magazine 135, 637–655.
Jordan, P.G., 1991. Development of asymmetric shale pull-apart in evaporite shear zones. Journal of Structural Geology 13, 399–409.
Karmakar, S., Mandal, N., 1989. Rotation and offset of shear fracture boudins. Indian Journal of Geology 61, 41–49.
Kidan, T.W., Cosgrove, J.W., 1996. The deformation of multilayers by layer-normal compression; an experimental investigation. Journal of Structural Geology 18, 461–474.
Ladeira, F.L., Price, N.J., 1981. Relationship between fracture spacing and bed thickness. Journal of Structural Geology 3, 179–183.
Lloyd, G.E., Ferguson, C.C., 1981. Boudinage structure—some new interpretations based on elastic–plastic finite element simulations. Journal of Structural Geology 3, 117–129.
Lloyd, G.E., Ferguson, C.C., Reading, K., 1982. A stress-transfer model for the development of extension fracture boudinage. Journal of Structural Geology 4, 355–372.
Lohest, M., 1909. Sur l'origine des veins et des geodes des terrians primaries de Belgique. Ann. Soc. Geol. Belgique 36B, 275–282.
Mandal, N., Karmakar, S., 1989. Boudinage in homogeneous foliated rocks. Tectonophysics 170, 151–158.
Mandal, N., Khan, D., 1991. Rotation, offset and separation of oblique-fracture (rhombic) boudins: theory and experiments under layer-normal compression. Journal of Structural Geology 13, 349–356.
Mandal, N., Deb, S.K., Khan, D., 1994. Evidence of a non-linear relationship between fracture spacing and layer thickness. Journal of Structural Geology 16, 1275–1281.
Masuda, T., Kuriyama, M., 1988. Successive "mid-point" fracturing during microboudinage: an estimate of the stress–strain relation during a natural deformation. Tectonophysics 147, 171–177.
Paterson, M.S., 1978. Experimental rock deformation. The brittle field. Springer-Verlag, New York.
Platt, J.P., Vissers, R.L., 1980. Extensional structures in anisotropic rocks. Journal of Structural Geology 2, 397–410.
Pollard, D.D., Segall, P., 1987. Theoretical displacements and stresses near fractures in rocks with applications to faults, joints, veins, dikes, and solution surfaces. In: Atkinson, B.K. (Ed.), Fracture Mechanics of Rocks. Academic Press, London, pp. 277–349.
Ramberg, H., 1955. Natural and experimental boudinage and pinch-and swell structures. Journal of Geology 63, 512–526.
Ramsay, J.G., Huber, M.I., 1987. The techniques of Modern Structural Geology. Volume 1: Strain Analysis. Academic Press, London.
Souffaché, B., Angelier, J., 1989. Distribution de joints de tension dans un banc rocheux: principe d'une mode'lisation energetique. Comptes Rendus de l'Academie des Sciences 308 (Serie II), 1385–1390.
Strömgard, K.E., 1973. Stress distribution during deformation of boudinage and pressure shadows. Tectonophysics 16, 215–248.
Talbot, C.J., 1970. The minimum strain ellipsoid using quartz veins. Tectonophysics 9, 47–76.
Uemura, T., 1965. Tectonic analysis of the boudin structure in the Muro group, Ku peninsula, southwest Japan. Journal of Earth Sciences 13, 99–144.
Wegmann, C.E., 1932. Note sur le boudinage. Bulletin of Geological Society of France Ser 5 11, 477–489.